

# Evaluation of Free Radical Scavenging Ability of Triazole-3-Thiol: A Combination of Experimental and Theoretical Approaches

Dinh Quy Huong,\* Pham Cam Nam, Duong Tuan Quang, Son Tung Ngo, Tran Duong, and Nguyen Minh Tam



Cite This: *ACS Omega* 2024, 9, 24071–24081



Read Online

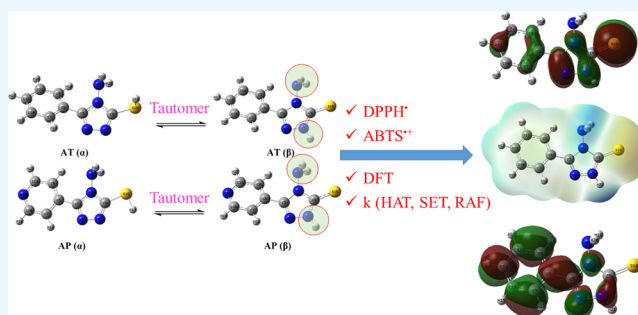
ACCESS |

Metrics & More

Article Recommendations

Supporting Information

**ABSTRACT:** An assessment of the free radical scavenging potential of 4-amino-5-phenyl-4H-1,2,4-triazole-3-thiol (AT) and 4-amino-5-(4-pyridyl)-4H-1,2,4-triazole-3-thiol (AP) involved a combination of experimental methodologies and theoretical calculations. In the 2,2-diphenyl-1-picrylhydrazyl (DPPH<sup>•</sup>) assay, AT exhibited an heightened efficacy in scavenging DPPH<sup>•</sup> radicals compared to AP. This was evidenced by the notably lower IC<sub>50DPPH</sub> value observed for AT ( $1.3 \times 10^{-3} \pm 0.2 \times 10^{-3}$  M) in comparison to AP ( $2.2 \times 10^{-3} \pm 0.1 \times 10^{-3}$  M). Similarly, in the 2,2'-azinobis(3-ethylbenzothiazoline-6-sulfonate) (ABTS<sup>•+</sup>) test, AT exhibited superior ability in neutralizing ABTS<sup>•+</sup> free radical cations compared to AP, with the computed IC<sub>50ABTS</sub> values of  $4.7 \times 10^{-5} \pm 0.1 \times 10^{-5}$  M for AT and  $5.5 \times 10^{-5} \pm 0.2 \times 10^{-5}$  M for AP. Density functional theory served as the tool for evaluating the correlation between structural attributes and the antioxidant efficacy of the studied molecules. The findings highlighted the flexibility of hydrogen atoms within NH and NH<sub>2</sub> groups to nucleophilic attacks, indicative of their pivotal role in the scavenging mechanism. Furthermore, investigations into the interactions between AT and AP with the free radical HOO<sup>•</sup> revealed predominantly the reaction via the hydrogen atom transfer mechanism. Both experimental observations and theoretical deductions collectively affirmed AT's superior free radical scavenging ability over AP in the gas phase and ethanol.



## 1. INTRODUCTION

Free radicals, characterized by one or more unpaired electrons, are inherently unstable chemical species known for their capability to induce cellular damage.<sup>1</sup> To counteract their harmful effects, antioxidants are widely employed to mitigate oxidative stress and protect cellular integrity.<sup>2</sup> The utilization of antioxidants spans in many various domains, including industrial materials preservation, food science,<sup>3</sup> and pharmaceutical applications.<sup>4</sup>

Triazole derivatives represent a class of heterocyclic compounds featuring a five-membered ring comprising two carbon and three nitrogen atoms.<sup>5</sup> Recent interest in these compounds, particularly within medicinal chemistry, stems from their diverse pharmacological properties, such as antiviral,<sup>6</sup> antimigraine,<sup>7</sup> anxiolytic, and antifungal effects.<sup>8</sup> Notably, 1,2,4-triazole and its derivatives exhibit significant biological activities, including antioxidant capabilities demonstrated through their ability to scavenge free radicals.<sup>8,9</sup>

An investigation conducted by Pokuri et al. involved the synthesis and assessment of twenty-six 1,2,4-triazole analogs, highlighting their exceptional potential as free radical scavengers through 2,2-diphenyl-1-picrylhydrazyl (DPPH<sup>•</sup>) assay.<sup>10</sup> The utilization of 2D-QSAR models correlated with the in vitro findings, elucidating the key structural attributes

prevalent in the molecules that contributed to their antioxidant efficacy. Similarly, Koparir et al. reported high DPPH<sup>•</sup> free radical scavenging efficiency of 4-substituted-5-(2-thienyl)-1,2,4-triazole-3-thione, surpassing typical antioxidants like ascorbic acid.<sup>11</sup>

Das and collaborators employed the structural template of 1,2,4-triazole and hydroxamic acid to synthesize 12 derivatives of 5-substituted-4-amino-1,2,4-triazole-linked hydroxamic acid.<sup>12</sup> Among these compounds, the synthesized derivative exhibited remarkable free radical scavenging potential, with IC<sub>50</sub> values of  $21.23 \times 10^{-6} \pm 8.51 \times 10^{-6}$  M in the DPPH<sup>•</sup> assay and  $15.32 \times 10^{-6} \pm 1.85 \times 10^{-6}$  M in the 2,2'-azinobis(3-ethylbenzothiazoline-6-sulfonate) (ABTS<sup>•+</sup>) assay. In a related study, Cetin and Gecibesler synthesized a series of phenol- and pyridine-substituted 1,2,4-triazole derivatives and assessed their antioxidant activity through various methods, including DPPH<sup>•</sup> and ABTS<sup>•+</sup> assays.<sup>13</sup> Compounds with

Received: March 27, 2024

Revised: May 8, 2024

Accepted: May 13, 2024

Published: May 21, 2024



electron-donating functional groups exhibited enhanced antioxidant capacity compared to electron-withdrawing groups, guiding the selection of electron-donating substituents for future antioxidant design.

Compounds such as 4-amino-5-phenyl-4H-1,2,4-triazole-3-thiol (AT) and 4-amino-5-(4-pyridyl)-4H-1,2,4-triazole-3-thiol (AP) featuring electron-repelling groups ( $-\text{NH}_2$ , SH) were identified as new potential free radical scavengers due to their structural characteristics. Their antioxidant capacities were evaluated using DPPH $\cdot$  and ABTS $\cdot^+$  assays, complemented by quantum chemical calculations to elucidate structural influences on the antioxidant activity.

Additionally, frontier molecular orbital analysis, global descriptors, and molecular electrostatic potential analysis were employed to characterize reactivity<sup>14</sup> and predict electrophilic and nucleophilic centers.<sup>15</sup> Thermodynamic parameters, including bond dissociation energy (BDE), ionization potential (IP), proton dissociation energy (PDE), proton affinity (PA), and electron transfer energy (ETE), served as valuable indicators for discerning active sites within a molecule and determining the favored mechanism of radical scavenging.<sup>16</sup> They were calculated under various environments to simulate experimental conditions, including gas phase and ethanol. Furthermore, a comparative analysis of free radical scavenging rates between AT, AP, and HOO $\cdot$  radicals was elucidated through the different mechanisms such as hydrogen abstract transfer (HAT), single electron transfer (SET), and radical adduct formation (RAF).<sup>17</sup>

## 2. METHODS

**2.1. Experimental Methods.** **2.1.1. Materials.** 4-Amino-5-phenyl-4H-1,2,4-triazole-3-thiol (AT) and 4-amino-5-(4-pyridyl)-4H-1,2,4-triazole-3-thiol (AP) were obtained from Merck, Germany. Their structures are presented in Figure 1. Absolute ethanol, 2,2-diphenyl-1-picrylhydrazyl, 2,2'-azinobis(3-ethylbenzothiazoline-6-sulfonic acid) diammonium salt, and  $\text{K}_2\text{S}_2\text{O}_8$  were obtained from Sigma-Aldrich.

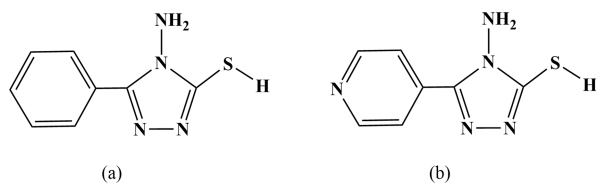


Figure 1. Molecular structures of (a) AT and (b) AP.

**2.1.2. Methods.** **2.1.2.1. 2,2-Diphenyl-1-picrylhydrazyl (DPPH $\cdot$ ) Assay.** The investigated 2,2-diphenyl-1-picrylhydrazyl (DPPH $\cdot$ ) solution was prepared by diluting it appropriately in ethanol to attain a concentration of  $6.7 \times 10^{-5}$  M.<sup>18</sup> To prevent photodecomposition, the solution was shielded from light using aluminum foil. Antioxidants were dissolved in ethanol across concentrations ranging from  $10^{-4}$  to  $10^{-3}$  M. Subsequently, the antioxidant solutions were mixed with the DPPH $\cdot$  solution at a volume ratio of 3:1. The resulting reaction mixtures were vigorously shaken and kept in darkness for 30 min, maintaining coverage with aluminum foil. Three repetitions were conducted for each experiment. The absorbance of the solutions was taken at 515 nm using a TCC-240A SHIMADZU UV/vis spectrophotometer. The ability to scavenge DPPH $\cdot$  free radicals ( $\text{SE}_{\text{DPPH}\cdot\%}$ ) was determined based on the absorbance, employing Formula 1:

$$\text{SE}_{\text{DPPH}\cdot\%} = \frac{A_b - A_s}{A_b} \times 100 \quad (1)$$

where  $A_b$  represents the absorbance of the blank (blank = 1 mL of DPPH $\cdot$  + 3 mL of ethanol) and  $A_s$  represents the absorbance of the investigated solution (sample = 1 mL of DPPH $\cdot$  + 3 mL of antioxidant at different concentrations).

**2.1.2.2. 2,2'-Azinobis(3-ethylbenzothiazoline-6-sulfonate) (ABTS $\cdot^+$ ) Assay.** The ABTS $\cdot^+$  assay was performed according to the modified protocol established by Re et al.<sup>19</sup> Initially, a stock solution of 2,2'-azinobis(3-ethylbenzothiazoline-6-sulfonic acid) diammonium salt (ABTS) was prepared in water with a concentration of  $7 \times 10^{-3}$  M. This ABTS stock solution was then mixed with 0.14 M  $\text{K}_2\text{S}_2\text{O}_8$  to generate a solution containing the green ABTS $\cdot^+$  free radical cation. The resulting mixture underwent a 16 h incubation period in darkness at room temperature to ensure a complete reaction. Following incubation, the reaction mixture was diluted with ethanol to achieve an absorbance of  $0.7 \pm 0.05$  on the spectrophotometer.

AT was diluted appropriately in ethanol to concentrations ranging from  $2 \times 10^{-5}$  to  $10^{-4}$  M, while AP was prepared at concentrations ranging from  $10^{-5}$  to  $3 \times 10^{-4}$  M. A combination of 1 mL of antioxidant solution and 3 mL of ABTS $\cdot^+$  free radical cation solution was prepared, with the reaction mixture covered with aluminum foil and incubated at room temperature for 6 min. The absorbance of the resulting mixture was measured at 734 nm using a TCC-240A SHIMADZU UV/vis spectrophotometer. Each experiment was replicated three times. The assessment of the capability to scavenge ABTS $\cdot^+$  free radical cations was determined based on the absorbance, employing Formula 2:

$$\text{SE}_{\text{ABTS}\cdot^+\%} = \frac{A'_b - A'_s}{A'_b} \times 100 \quad (2)$$

where  $A'_b$  control represents the absorbance of the blank (blank = 3 mL of ABTS $\cdot^+$  + 1 mL of ethanol), and  $A'_s$  represents the absorbance of the sample (sample = 3 mL of ABTS $\cdot^+$  + 1 mL of antioxidant at different concentrations).

**2.2. Quantum Chemical Calculations.** Gaussian 16 software<sup>20</sup> was utilized to perform density functional theory (DFT) calculations using the M06-2X/6-311++G(d,p) level of theory.<sup>21</sup> This theoretical level was chosen to optimize the molecular structures under investigation and compute various thermodynamic parameters and rate constants. In this study, ethanol was selected to simulate experimental conditions. The influence of ethanol as a solvent was approximated using the SMD solvation model.<sup>22</sup> Global descriptive parameters such as the highest occupied molecular orbital energy ( $E_{\text{HOMO}}$ ), lowest unoccupied molecular orbital energy ( $E_{\text{LUMO}}$ ), frontier molecular orbital gap ( $\Delta E_{\text{L-H}}$ ), hardness ( $\eta$ ),<sup>23</sup> and electro-negativity ( $\chi$ ) were calculated using the following formulas<sup>24</sup>:

$$\Delta E_{\text{L-H}} = E_{\text{LUMO}} - E_{\text{HOMO}} \quad (3)$$

$$\text{IE} = -E_{\text{HOMO}} \quad (4)$$

$$\text{EA} = -E_{\text{LUMO}} \quad (5)$$

$$\eta = \frac{\text{IE} - \text{EA}}{2} = \frac{E_{\text{LUMO}} - E_{\text{HOMO}}}{2} \quad (6)$$

$$\chi = \frac{\text{IE} + \text{EA}}{2} = -\frac{(E_{\text{HOMO}} + E_{\text{LUMO}})}{2} \quad (7)$$

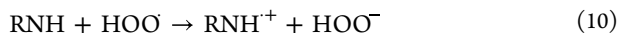
The hydrogen atom transfer (HAT) mechanism depends on the pivotal exchange of hydrogen atom from the antioxidant molecule to the free radical. This process is assessed by the bond dissociation enthalpy (BDE).<sup>25</sup>



The BDE of RNH is calculated as follows:

$$\text{BDE}(\text{RNH}) = \text{H}(\text{H} \cdot) + \text{H}(\text{RN} \cdot) - \text{H}(\text{RNH}) \quad (9)$$

In the case of the sequential electron transfer proton transfer (SET-PT) mechanism, two steps are involved<sup>26</sup>:



These steps correspond to the thermodynamic parameters as ionization potential (IP) and proton affinity (PA), calculated as<sup>27</sup>

$$\text{IP} = \text{H}(\text{RNH}^{\cdot+}) + \text{H}(\text{e}^-) - \text{H}(\text{RNH}) \quad (12)$$

$$\text{PDE} = \text{H}(\text{RN} \cdot) + \text{H}(\text{H}^+) - \text{H}(\text{RNH}^{\cdot+}) \quad (13)$$

For the sequential proton-loss electron transfer (SPLET) mechanism<sup>28</sup>:



Proton affinity (PA) and electron transfer enthalpy (ETE) are two critical parameters for SPLET,<sup>29</sup> calculated as

$$\text{PA} = \text{H}(\text{RN}^-) + \text{H}(\text{H}^+) - \text{H}(\text{RNH}) \quad (16)$$

$$\text{ETE} = \text{H}(\text{RN} \cdot) + \text{H}(\text{e}^-) - \text{H}(\text{RN}^-) \quad (17)$$

where RNH represents AT and AP. The enthalpies of each species at 298 K are represented by H. The study results of Marković et al. provided the enthalpies of the electron and proton in the gas phase and those in ethanol.<sup>30</sup>

In addition to thermodynamic parameters, the reactivity of antioxidants and free radicals also depends on their reaction rate (*k*). Table S1 provides detailed instructions on calculating the rate constants for the HAT,<sup>31</sup> SET,<sup>32</sup> and RAF mechanisms.<sup>33</sup>

The proportions of products (*P*%) produced by various reaction mechanisms were approximated utilizing eqs 18–20.<sup>34</sup>

$$P_{\text{HAT}}\% = \frac{k_{\text{HAT}}}{k_{\text{tot}}} \times 100 \quad (18)$$

$$P_{\text{SET}}\% = \frac{k_{\text{SET}}}{k_{\text{tot}}} \times 100 \quad (19)$$

$$P_{\text{RAF}}\% = \frac{k_{\text{RAF}}}{k_{\text{tot}}} \times 100 \quad (20)$$

### 3. RESULTS AND DISCUSSION

**3.1. DPPH<sup>•</sup> Free Radical Scavenging Assay.** The DPPH<sup>•</sup> assay, reliant on the stable free radical 2,2-diphenyl-1-picrylhydrazyl, offers an efficient method for assessing antioxidant activity.<sup>35</sup> This stable radical, characterized by an unpaired valence electron at a nitrogen bridge, imparts a violet hue to its ethanol solution. Upon interacting with an antioxidant, DPPH<sup>•</sup> free radicals undergo reduction, resulting

in the formation of yellow diphenylpicrylhydrazine.<sup>36</sup> UV–vis spectrophotometric analysis of the change in optical density reveals the efficacy of antioxidants in scavenging DPPH<sup>•</sup> radicals. As depicted in Figure 2, variations in absorbance

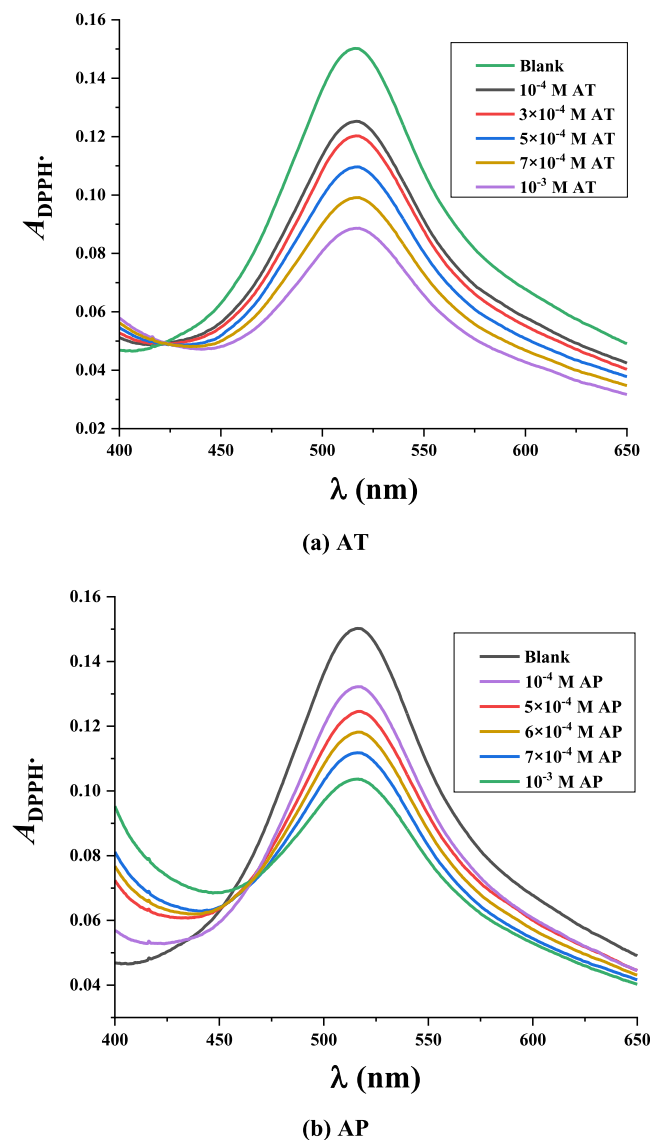
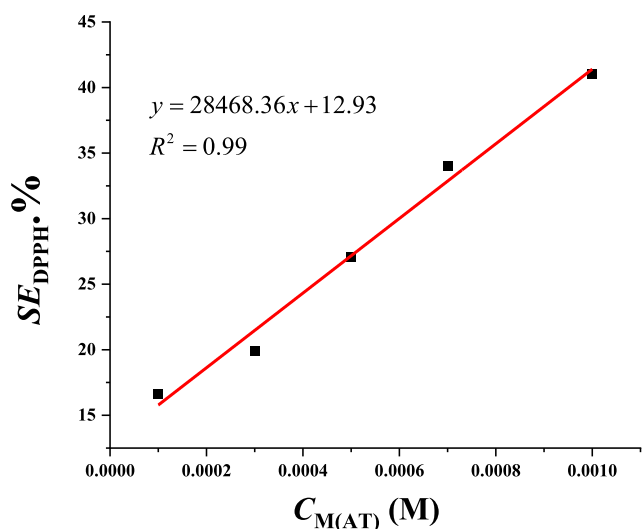


Figure 2. UV–vis spectra of (a) AT and (b) AP in DPPH<sup>•</sup> assay.

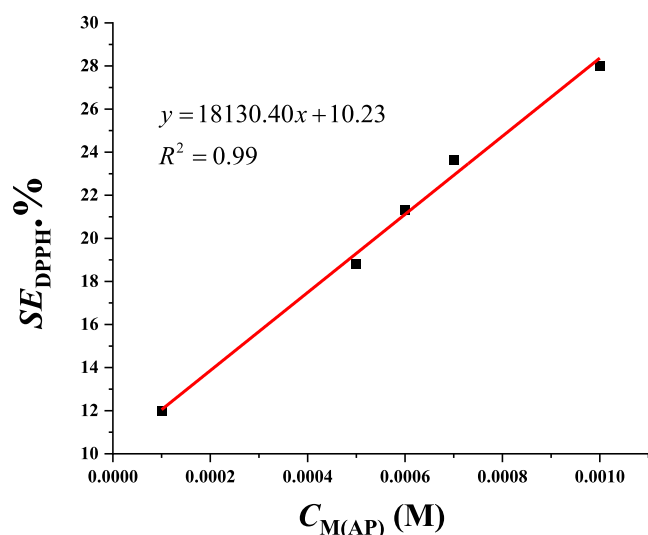
correlate with the concentrations of antioxidants AT and AP. Higher concentrations of antioxidants correspond to diminished absorbance, indicating greater scavenging activity.

The assessment of DPPH<sup>•</sup> scavenging ability is quantified through IC<sub>50DPPH</sub> values, representing the sample concentration necessary to inhibit 50% of the initial DPPH<sup>•</sup> concentration.<sup>37</sup> Calculations based on the relationship between scavenging efficiency and concentrations of AT and AP (as illustrated in Figure 3) yield IC<sub>50DPPH</sub> values of  $1.3 \times 10^{-3} \pm 0.2 \times 10^{-3}$  M for AT and  $2.2 \times 10^{-3} \pm 0.1 \times 10^{-3}$  M for AP, respectively. This suggests a stronger DPPH<sup>•</sup> capturing capacity for AT compared to AP.

**3.2. 2,2'-Azino-bis(3-ethylbenzothiazoline-6-sulfonate) (ABTS<sup>•+</sup>) Free Radical Cation Scavenging Assay.** The antioxidant potential of AT and AP is evaluated using the ABTS<sup>•+</sup> assay, wherein 2,2'-azino-bis(3-ethylbenzothiazoline-



(a) AT

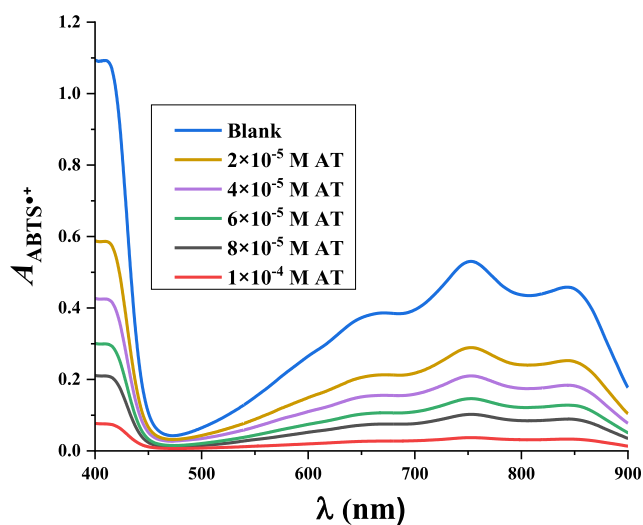


(b) AP

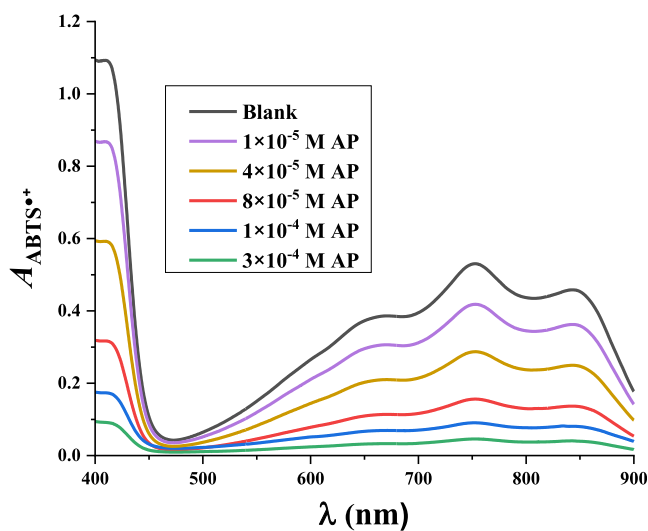
**Figure 3.** Relationship between the DPPH $\cdot$  scavenging efficiency and concentrations of (a) AT and (b) AP.

6-sulfonic acid) (ABTS) is oxidized to its radical cation ABTS $\cdot^+$  upon reaction with potassium persulfate, resulting in a blue-colored solution ( $\lambda_{max} = 734 \text{ nm}$ ). Upon interaction with antioxidants, the ABTS $\cdot^+$  radical cation is depleted, causing the solution to transition from blue to colorless.

Ultraviolet–visible spectra of ABTS $\cdot^+$  at varying concentrations of AT and AP are depicted in Figure 4. Analogous to the DPPH $\cdot$  assay, increasing concentrations of AT and AP correlate with diminishing spectral intensity, indicating a reduction in solution absorbance and, hence, a decrease in ABTS $\cdot^+$  concentration.  $IC_{50ABTS}$  values for AT and AP are derived from graphs illustrating the relationship between ABTS $\cdot^+$  scavenging efficiency ( $SE_{ABTS\cdot^+}$ ) and antioxidant concentrations (Figure 5). AT exhibits an  $IC_{50ABTS}$  value of  $4.7 \times 10^{-5} \pm 0.1 \times 10^{-5} \text{ M}$ , while AP demonstrates a value of  $5.5 \times 10^{-5} \pm 0.2 \times 10^{-5} \text{ M}$ . These findings underscore AT's superior ability to neutralize ABTS $\cdot^+$  radical cations compared to AP. Consequently, both experimental methodologies



(a) AT

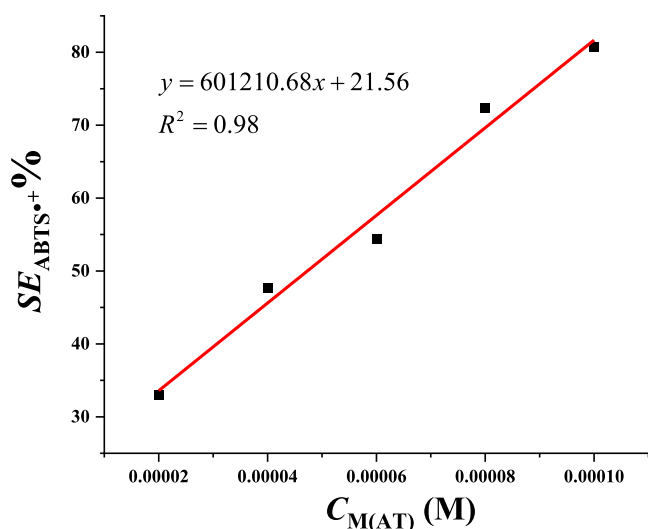


(b) AP

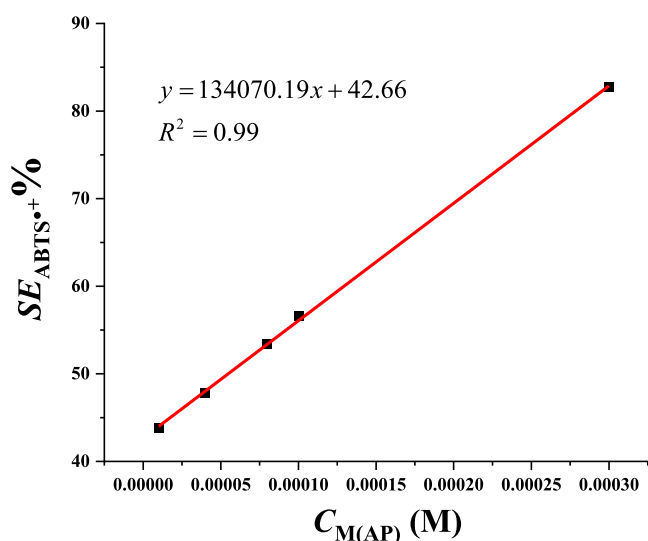
**Figure 4.** UV–vis spectra of (a) AT and (b) AP in ABTS $\cdot^+$  assay.

(DPPH $\cdot$  and ABTS $\cdot^+$ ) affirm AT's efficacy in quenching free radicals relative to AP.

**3.3. Computational Results.** Due to the structural characteristics of the SH bond in AT and AP molecules, they exhibit different tautomeric forms. Consequently, all possible geometries of tautomers, denoted as forms ( $\alpha$ ) and ( $\beta$ ), were explored for AT and AP, as depicted in Figure 6. In these molecules, the hydrogen atom of the SH group demonstrates a tendency to migrate to nitrogen atom N3 in AT and AP molecules. The geometric configurations of all tautomers of AT and AP were optimized utilizing the M06-2X/6-311++G(d,p) level of theory. Cartesian coordinates for the species in the gas phase and ethanol are provided in Tables S2–S5 of the Supplementary Data. Energy calculations for the tautomers of AT and AP indicate that form ( $\beta$ ) exhibits greater stability than form ( $\alpha$ ). Moreover, the validation of the bond compositions of AT and AP was accomplished through an exhaustive analysis of their infrared (IR) spectra, as delineated in Figure S1. Consequently, AT and AP's form ( $\beta$ ) are selected for further research.



(a) AT



(b) AP

Figure 5. Relationship between the ABTS<sup>•+</sup> scavenging efficiency and concentrations of (a) AT and (b) AP.

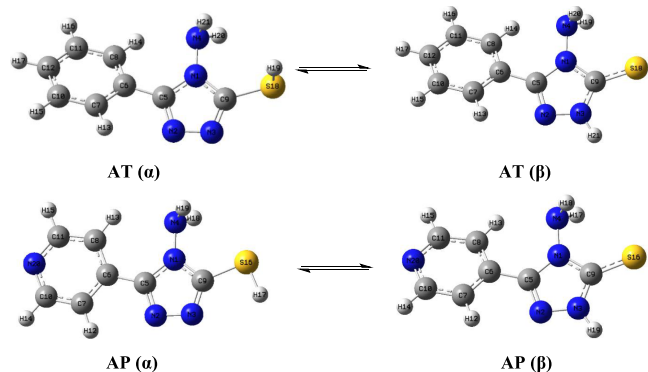


Figure 6. Tautomers of AT and AP at M06-2X/6-311++G(d,p).

**3.3.1. Frontier Molecular Orbitals and Reactivity Descriptors.** Frontier molecular orbitals were analyzed to gain insight into the chemical reactivity of the molecules.<sup>38</sup> Figure 7

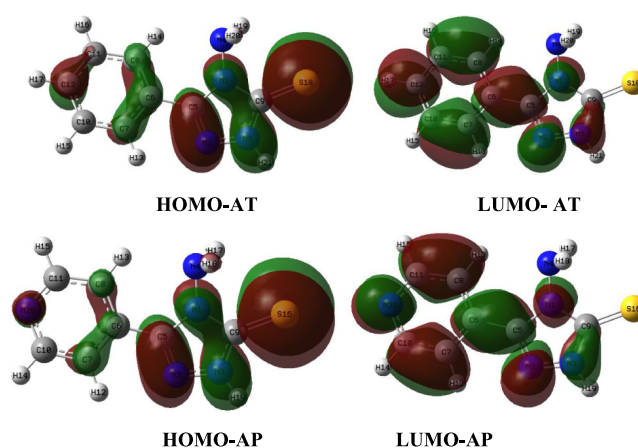


Figure 7. HOMO and LUMO molecular orbital plots for AT and AP in the gas phase.

illustrates the electron density distribution of the highest occupied molecular orbital (HOMO) and the lowest unoccupied molecular orbital (LUMO) for AT and AP molecules in the gas phase. Electron transfer zones are predominantly distributed throughout the molecules for both AT and AP. This suggests that free radicals can attack various sites in both AT and AP molecules, including aromatic rings, NH, and NH<sub>2</sub> groups. The HOMO plots may indicate active sites for free radical elimination through hydrogen abstraction after electron transfer.<sup>39</sup>

The  $E_{\text{HOMO}}$  values, rather than  $E_{\text{LUMO}}$  values, can indicate scavenging activities.<sup>40</sup> AT and AP exhibit  $E_{\text{HOMO}}$  values of  $-7.22$  and  $-7.48$  eV in the gas phase, and  $-7.27$  and  $-7.37$  eV in ethanol, respectively, suggesting that AT may scavenge free radicals more effectively than AP in both environments.

The energy gap between these orbitals, resulting in greater polarizability of the molecule, is typically associated with higher chemical reactivity and lower kinetic stability. Studies suggest that molecules with a lower frontier molecular orbital gap ( $\Delta E_{\text{L-H}}$ ) are more polarized.<sup>41</sup> As presented in Table 1, AT

Table 1. Global Reactivity Descriptors of Studied Antioxidants at M06-2X/6-311++G(d,p)

phase	compounds	$E_{\text{HOMO}}$ (eV)	$E_{\text{LUMO}}$ (eV)	$\Delta E_{\text{L-H}}$ (eV)	$\eta$ (eV)	$\chi$ (eV)
gas	AT	$-7.22$	$-0.93$	$6.29$	$3.15$	$4.07$
	AP	$-7.48$	$-1.05$	$6.43$	$3.21$	$4.26$
ethanol	AT	$-7.27$	$-0.55$	$6.72$	$3.36$	$3.91$
	AP	$-7.37$	$-0.54$	$6.83$	$3.41$	$3.95$

demonstrates a lower  $\Delta E_{\text{L-H}}$  value ( $6.29$  eV in the gas phase and  $6.72$  eV in ethanol) compared to AP, indicating higher polarizability and a stronger tendency to react with free radicals.<sup>42</sup> Additionally, hardness ( $\eta$ ), a global descriptive parameter directly linked to molecule stability, was computed to provide deeper insights into the reactive nature of the studied derivatives.<sup>43</sup> AT exhibits hardness values of  $3.15$  eV in the gas phase and  $3.36$  eV in ethanol, while those of AP are  $3.21$  and  $3.41$  eV in the gas phase and ethanol, respectively. This suggests that AT is more prone to react with free radicals than AP.

Considering the charge-transfer reaction, electronegativity ( $\chi$ ) is key parameter to analyze the antioxidant activity of a compound.<sup>44</sup> Lower electronegativity values indicate a

molecule's capability to donate electrons. AT, with lower  $\chi$  values (4.07 eV in the gas phase and 3.91 eV in ethanol), exhibits good electron-donating tendencies among the studied derivatives. Moreover, the lower electronegativity values in ethanol compared to the gas phase suggest that electron transfer reactions occur more readily in ethanol.

Overall, global reactivity descriptor values indicate that AT exhibits better potential as an antioxidant than AP in both the gas phase and ethanol.

**3.3.2. Molecular Electrostatic Potential.** Molecular electrostatic potential analysis has been employed to elucidate the reactivity patterns of the investigated derivatives.<sup>45</sup> Regions exhibiting a red coloration denote negatively charged zones, indicative of favorable electrophilic attack.<sup>46</sup> Conversely, blue-colored regions signify positive electrostatic potential, which attracts radical species.<sup>47</sup> Notably, nitrogen atom within a six-membered ring of AP and sulfur atoms in AT and AP molecules exhibit elevated electrostatic potential, while hydrogen atoms within the amine ( $-\text{NH}_2$  and  $-\text{NH}$ ) groups manifest lower electrostatic potential (Figure 8). In other words, the  $-\text{NH}_2$  and  $-\text{NH}$  groups in AT and AP molecules are predominant positions for the attack of free radicals.

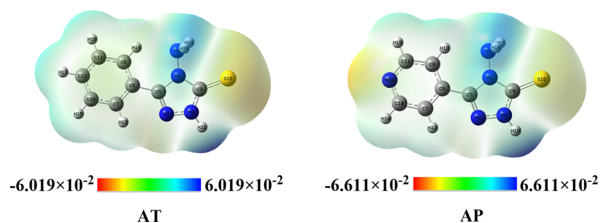


**Figure 8.** Molecular electrostatic potential of the investigated derivatives.

**3.3.3. Thermodynamic Parameters of AT and AP in the Gas Phase and Ethanol.** Crucial thermodynamic parameters for understanding molecular reactivity encompass bond dissociation energy (BDE), ionization potential (IP), proton dissociation energy (PDE), proton affinity (PA), and electron transfer energy (ETE).<sup>48</sup> These parameters support to elucidate three main reaction mechanisms: hydrogen atom transfer (HAT), electron transfer proton transfer (SET-PT), and proton transfer electron transfer (SPLET).<sup>49</sup> In examining the N–H bonds within the  $\text{NH}_2$  group of AT and AP, it is important to note their structural similarity, wherein only one N–H bond within this group is assessed.

Within the context of the HAT mechanism, a free radical initiates isomeric cleavage, leading to the separation of a hydrogen atom from either the  $\text{NH}_2$  or  $\text{NH}$  group. This process is relevant in assessing a compound's antioxidant ability, with lower BDE values indicating heightened antioxidant activity. Notably, upon observing Table 2, it is observed that the BDE values of the N4–H bonds consistently yield smaller values than those of BDE(N3–H) across both gas and ethanol environments. This observation suggests that the hydrogen atom transfer reaction occurs more efficiently at the N4–H positions than at the N3–H positions.

The antioxidant efficacy of AT and AP may vary depending on the environmental conditions of the study. Analysis from Table 2 reveals that the hydrogen-supplying ability in ethanol is comparatively inferior to that in a gas phase. Specifically, in ethanol, the BDE values of N4–H20, and N3–H21 bonds in AT are recorded at 86.8 and 88.8 kcal mol<sup>-1</sup>, respectively,

**Table 2.** Thermodynamic Parameters of AT and AP in the Gas Phase and Ethanol

thermodynamic parameters (kcal mol <sup>-1</sup> )	compounds	positions	gas	ethanol
BDE	AT	N4–H20	86.8	90.7
		N3–H21	88.8	90.1
	AP	N4–H17	87.1	90.9
		N3–H19	89.6	90.9
IP	AT		182.8	127.2
	AP		190.2	129.5
PDE	AT	N4–H20	217.3	7.0
		N3–H21	219.3	6.3
	AP	N4–H17	210.3	4.9
		N3–H19	212.8	4.8
PA	AT	N4–H20	350.8	54.8
		N3–H21	331.8	33.0
	AP	N4–H17	345.5	52.9
ETE	AT	N4–H20	49.3	79.3
		N3–H21	70.3	100.5
	AP	N4–H17	55.0	81.5
		N3–H19	76.5	102.8

whereas for AP, the corresponding N4–H17 and N3–H19 bonds exhibit BDE values of 87.1 and 89.6 kcal mol<sup>-1</sup>. Consequently, BDE values are elevated in ethanol relative to the gas phase. Furthermore, all BDE values within AT are lower than those of AP, underscoring AT's proficiency as a free radical scavenger compared to AP, particularly under the HAT mechanism.

In the context of the SET-PT mechanism, the electron transfer ability is quantitatively evaluated through ionization potential (IP) value. IP values of AT and AP are 182.8 and 190.2 kcal mol<sup>-1</sup> in the gas phase; 127.2 and 129.5 kcal mol<sup>-1</sup> in ethanol, respectively. IP values decrease as the polarity of the solvent increases, indicating facilitated electron removal in polar solvents.

PDE determines the deprotonation properties of molecules. The PDE values of AT and AP in the gas and ethanol are summarized in Table 2. The N4–H20 bond of AT and the N4–H17 bond of AP are the two positions with the lowest PDE in the gas phase with values of 217.3 and 210.3 kcal mol<sup>-1</sup>. In ethanol, the PDE values decrease significantly due to the high solvation enthalpy of the proton. Specifically, PDE values of the N4–H20 bond in AT and N4–H17 in AP are 7.0 and 4.9 kcal mol<sup>-1</sup> in ethanol.

According to the SPLET mechanism, the PA and ETE of AT and AP are considered. As seen in Table 2, the PA of AT has values of 350.8 and 331.8 kcal mol<sup>-1</sup>, which correspond to the N4–H20 and N3–H21 bonds in the gas phase. These values of AP are 345.5 and 326.4 kcal mol<sup>-1</sup>, which corresponds to N4–H17 and N3–H19 positions. PA values decrease from 296.0–298.8 kcal mol<sup>-1</sup> for AT and 292.6–294.9 kcal mol<sup>-1</sup> for AP in ethanol. The trend of decreasing PA from gas to solvent medium with increasing polarity indicates that polar solvents facilitate deprotonation.<sup>50</sup>

ETE is the following thermodynamic parameter to be evaluated in the SPLET mechanism when electron transfer proceeds from the deprotonated radical. As indicated in Table 2, the ETE values for both compounds are higher in the ethanol solvent than in the gas environment. Remarkably, the ETE of the proton radical is lower than the IP of the neutral

molecule, suggesting that electron transfer is more facile from the deprotonated form than from the neutral form.

The three mechanisms, HAT, SET-PT, and SPLET, are predominantly characterized by distinct thermodynamic parameters: BDE, IP, and PA, respectively.<sup>51</sup> Notably, the IP and PA values in the gas phase exceed the BDE values of AT and AP, whereas, in ethanol, PA is lower than the corresponding BDE and IP values. Consequently, the HAT mechanism is thermodynamically favored in the gas phase, while the SPLET mechanism finds preference in polar media for both investigated compounds.

**3.3.4. Kinetic Study for the Reaction between AT, AP, and  $\text{HOO}^\bullet$ .** The assessment of thermodynamic parameters plays a crucial role in determining the feasibility of chemical processes. However, confirming an antioxidant's potency requires a comprehensive evaluation beyond thermodynamics. For an antioxidant to be deemed efficacious, it must exhibit rapid reactivity toward free radicals. Thus, the rate constants of reactions between AT and AP with free radicals are investigated, employing the M06-2X/6-311++G(d,p) methodology in both the gas phase and ethanol solvent with different mechanisms.

$\text{HOO}^\bullet$  is a pivotal intermediate species in numerous chemical reactions, characterized by its relatively prolonged lifespan and ability to diffuse into adjacent structures.<sup>52</sup> In this investigation,  $\text{HOO}^\bullet$  is selected as a representative free radical for probing the rate constants.

Given the relatively low bond dissociation energy (BDE) values of the N–H bonds in AT and AP molecules, the hydrogen atom transfer (HAT) mechanism emerges as the primary focus. Upon interaction with  $\text{HOO}^\bullet$  radicals, these molecules undergo a sequential process, initiating with the formation of intermediate 1 (Inter 1), followed by the transition state (TS), and subsequent transformation into intermediate 2 (Inter 2).<sup>53</sup> Ultimately, the reaction yields products such as  $\text{HOOH}$  and a newly formed stable radical.

Figure 9 illustrates the potential energy surfaces of AT and AP in the gas phase across all reaction sites. It is evident that the reaction paths of both compounds with  $\text{HOO}^\bullet$  exhibit a comparable trend. Specifically, in the case of AT and  $\text{HOO}^\bullet$  reactions, the relative energy (relative to the reactants) of Inter 1 is calculated with values of  $-12.6$  and  $-13.9$  kcal mol<sup>-1</sup>; TS is represented by values of  $7.3$  and  $12.5$  kcal mol<sup>-1</sup>; Inter 2 by values of  $-6.5$  and  $-5.1$  kcal mol<sup>-1</sup>; and the product by values of  $1.5$  and  $3.5$  kcal mol<sup>-1</sup>, respectively, at the bonds linking N4–H20, and N3–H21. Notably, these bond values in the AP molecule appear to be higher in comparison to those of AT. For instance, the N4–H17 bond in AP exhibits respective values of  $-12.2$ ,  $7.9$ ,  $-6.3$ , and  $1.8$  kcal mol<sup>-1</sup>. Similarly, the N3–H19 bond presents relative values of  $-13.6$ ,  $12.8$ ,  $-4.3$ , and  $4.3$  kcal mol<sup>-1</sup>.

Based on conventional transition-state theory (TST) and Eyringpy software,<sup>54</sup> the rate constants of the reactions between AT and AP with  $\text{HOO}^\bullet$  at the active sites are calculated in Table 3. For AT, the rate constants at positions N4–H20, and N3–H21 are  $8.43 \times 10^3$  and  $3.13 \times 10^4$  M<sup>-1</sup> s<sup>-1</sup>, respectively. In contrast, for AP, the rate constants at positions N4–H17, and N3–H19 exhibit the values of  $3.07 \times 10^3$  and  $2.95 \times 10^4$  M<sup>-1</sup> s<sup>-1</sup>, respectively. Consequently, in the gas phase, the total rate constants according to the hydrogen atom transfer (HAT) mechanism are  $4.82 \times 10^4$  M<sup>-1</sup> s<sup>-1</sup> for AT and  $3.56 \times 10^4$  M<sup>-1</sup> s<sup>-1</sup> for AP, respectively. In ethanol, the rate constant values tend to decrease, potentially attributable to

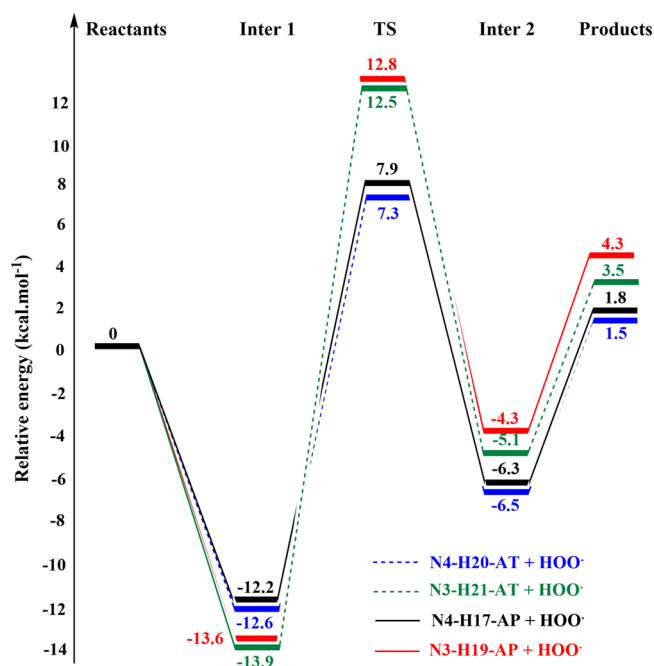
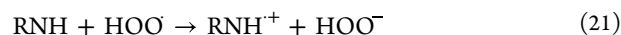


Figure 9. Potential energy surfaces of the reactions involving AT, AP, and  $\text{HOO}^\bullet$  under the HAT mechanism.

the influence of solvent molecules. AT yields a total rate constant of  $1.25 \times 10^2$  M<sup>-1</sup> s<sup>-1</sup>, whereas the corresponding value for AP is represented by  $2.26 \times 10^1$  M<sup>-1</sup> s<sup>-1</sup>. According to the HAT reaction mechanism in both the gas and ethanol phases, AT can react with  $\text{HOO}^\bullet$  faster than AP.

SET is the following mechanism applied to evaluate the antioxidant ability of AT and AP in the gas phase and ethanol. The processes of giving electron (Reaction 21) of the studied antioxidants and  $\text{HOO}^\bullet$  can occur as follows:



Gibbs free energies ( $\Delta G^\circ$ ), enthalpies ( $\Delta H^\circ$ ), and rate constants at 298.15 K for the single electron transfer (SET) reactions of AT and AP in the gas phase and ethanol are presented in Table 4. Notably, the electron-donating reactions of both AT and AP are established as endothermic, as evidenced by  $\Delta G^\circ$  and  $\Delta H^\circ$  values of  $159.80$  kcal mol<sup>-1</sup> and  $160.05$  kcal mol<sup>-1</sup> for AT, and  $167.00$  kcal mol<sup>-1</sup> and  $167.39$  kcal mol<sup>-1</sup> for AP, respectively (refer to Table 4). The comparison based on the  $\Delta G^\circ$  value suggests that the electron donation reaction of AT is more favorable than that of AP. It is worth noting that in ethanol solvent, both  $\Delta G^\circ$  and  $\Delta H^\circ$  values for AT and AP demonstrate significant decreases, indicating a preference for electron donation in the solvent phase over the gas phase.

Furthermore, utilizing Marcus' theory,<sup>32</sup> the determination of rate constant for the electron exchange reaction ( $k_{\text{SET}}$ ) is presented in Table 4. The findings indicate a minimal occurrence of the electron-donating reaction for AT and AP in the gas phase, contrasting with more favorable kinetics observed in ethanol, where rate constant values are calculated as  $1.90 \times 10^{-70}$  M<sup>-1</sup> s<sup>-1</sup> for AT and  $6.08 \times 10^{-111}$  M<sup>-1</sup> s<sup>-1</sup> for AP. These findings underscore AT's superior ability to donate electrons to  $\text{HOO}^\bullet$  compared to AP, and the reactions of both compounds with  $\text{HOO}^\bullet$  are more favorable in ethanol under the SET mechanism.

Table 3. Rate Constants of Reactions according to the HAT Mechanism for AT and AP in the Gas Phase and Ethanol

compounds	bonds	gas		ethanol	
		$k_{\text{HAT}(i)}$ ( $\text{M}^{-1} \text{s}^{-1}$ )	$k_{\text{HAT}}$ ( $\text{M}^{-1} \text{s}^{-1}$ )	$k_{\text{HAT}(i)}$ ( $\text{M}^{-1} \text{s}^{-1}$ )	$k_{\text{HAT}}$ ( $\text{M}^{-1} \text{s}^{-1}$ )
AT	N4–H20	$8.43 \times 10^3$	$4.82 \times 10^4$	3.20	$1.25 \times 10^2$
	N3–H21	$3.13 \times 10^4$		$1.19 \times 10^2$	
AP	N4–H17	$3.07 \times 10^3$	$3.56 \times 10^4$	$2.03 \times 10^{-1}$	$2.26 \times 10^1$
	N3–H19	$2.95 \times 10^4$		$2.21 \times 10^1$	

Table 4. Gibbs Free Energies, Enthalpies, and Rate Constants at 298.15 K for the SET Reactions of AT and AP in the Gas Phase and Ethanol

phase	compounds	$\Delta G^\circ$ ( $\text{kcal mol}^{-1}$ )	$\Delta H^\circ$ ( $\text{kcal mol}^{-1}$ )	$k_{\text{SET}}$ ( $\text{M}^{-1} \text{s}^{-1}$ )
gas	AT	159.80	160.05	$2.10 \times 10^{-489}$
	AP	167.00	167.39	$1.10 \times 10^{-533}$
ethanol	AT	40.30	40.62	$1.90 \times 10^{-70}$
	AP	42.80	42.95	$6.08 \times 10^{-111}$

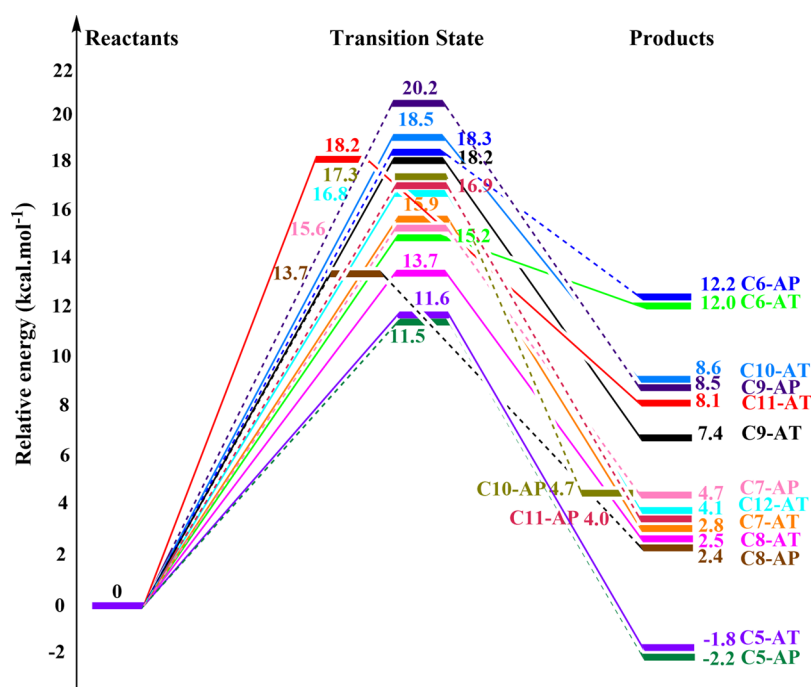
Figure 10. Potential energy surfaces of the reactions involving AT, AP, and  $\text{HOO}^\bullet$  under the RAF mechanism.

Table 5. Rate Constants of Reactions according to the RAF Mechanism for AT and AP in the Gas Phase and Ethanol

compounds	positions	gas		ethanol		
		$k_{\text{RAF}(i)}$ ( $\text{M}^{-1} \text{s}^{-1}$ )	$k_{\text{RAF}}$ ( $\text{M}^{-1} \text{s}^{-1}$ )	$k_{\text{RAF}(i)}$ ( $\text{M}^{-1} \text{s}^{-1}$ )	$k_{\text{RAF}}$ ( $\text{M}^{-1} \text{s}^{-1}$ )	
AT	C5	$9.63 \times 10^{-4}$	$1.00 \times 10^{-3}$	$5.00 \times 10^{-6}$	$6.35 \times 10^{-6}$	
	C6	$6.02 \times 10^{-7}$		$1.3 \times 10^{-8}$		
	C7	$2.95 \times 10^{-6}$		$7.20 \times 10^{-7}$		
	C8	$2.17 \times 10^{-5}$		$3.00 \times 10^{-7}$		
	C9	$1.20 \times 10^{-8}$		$1.60 \times 10^{-11}$		
	C10	$3.49 \times 10^{-6}$		$2.40 \times 10^{-8}$		
	C11	$7.22 \times 10^{-6}$		$4.20 \times 10^{-8}$		
	C12	$1.38 \times 10^{-6}$		$1.20 \times 10^{-7}$		
	AP	C5	$9.63 \times 10^{-4}$	$9.82 \times 10^{-4}$	$4.10 \times 10^{-6}$	$5.01 \times 10^{-6}$
		C6	$3.79 \times 10^{-9}$		$3.90 \times 10^{-11}$	
		C7	$2.95 \times 10^{-6}$		$5.20 \times 10^{-7}$	
		C8	$1.51 \times 10^{-5}$		$2.90 \times 10^{-7}$	
C9		$3.73 \times 10^{-10}$		$3.10 \times 10^{-13}$		
C11		$3.19 \times 10^{-7}$		$5.80 \times 10^{-8}$		

The investigation delves into the mechanism underlying the addition reaction between AT and AP with the free radical  $\text{HOO}^\bullet$ , focusing on the respective pi bonds in their molecular structures.<sup>55</sup> Specifically, the involvement of the  $\text{HOO}^\bullet$  radical in the RAF reaction with these antioxidants occurs at positions C5, C6, C7, C8, C9, C10, C11, and C12 (AT only). Figure 10 illustrates the potential energy surfaces of RAF reactions involving reactants, transition state formation, and products in the gas phase. Notably, reactions of AT with  $\text{HOO}^\bullet$  in the gas phase exhibit relative TS energies of 11.6, 15.2, 15.9, 13.7, 18.2, 18.5, 18.2, and 16.8 kcal mol<sup>-1</sup> (compared to the reactants) corresponding to positions C5, C6, C7, C8, C9, C10, C11, and C12. Conversely, the RAF reaction at positions C5, C6, C7, C8, C9, C10, and C11 of AP yields relative TS values of 11.6, 18.3, 15.6, 13.7, 20.2, 17.3, and 16.9 kcal mol<sup>-1</sup>, respectively. Notably, C5 exhibits the lowest surface potential in the gas phase for the reaction of AT and AP with  $\text{HOO}^\bullet$ , according to the RAF mechanism.

Using Eyringpy software, the rate constant values are calculated for gas and ethanol phases (Table 5) based on the potential energy surfaces of the reactions between AT and AP with  $\text{HOO}^\bullet$  via the RAF mechanism. In the gas phase, AT exhibits a total rate constant value of  $1.00 \times 10^{-3} \text{ M}^{-1} \text{ s}^{-1}$ , while in ethanol, it decreases to  $6.35 \times 10^{-6} \text{ M}^{-1} \text{ s}^{-1}$ . Similarly, AP demonstrates lower rate constant values than AT in both environments, specifically  $9.82 \times 10^{-4}$  and  $5.01 \times 10^{-6} \text{ M}^{-1} \text{ s}^{-1}$ , respectively. Notably, C5 remains the position yielding the most significant rate constant value for AT and AP. The findings suggest that AT reacts with the  $\text{HOO}^\bullet$  radical via the RAF mechanism more rapidly than AP.

Applying Formulas 18–20, the quantities of products generated via hydrogen atom transfer (HAT), single electron transfer (SET), and radical adduct formation (RAF) mechanisms are computed and outlined in Table 6. Notably,

**Table 6. Product Amounts of Reactions between AT and AP with  $\text{HOO}^\bullet$  According to Various Mechanisms**

phase	mechanism	AT	AP
gas	$P_{\text{HAT}}\%$	99.99%	99.99%
	$P_{\text{SET}}\%$	0.00%	0.00%
	$P_{\text{RAF}}\%$	0.01%	0.01%
ethanol	$P_{\text{HAT}}\%$	99.99%	99.99%
	$P_{\text{SET}}\%$	0.00%	0.00%
	$P_{\text{RAF}}\%$	0.01%	0.01%

the product yield from AT through the HAT mechanism in the gas phase and ethanol solution constitutes 99.99% of the total product. On the contrary, the contribution of products from the SET and RAF mechanisms is nearly insignificant. This trend is similar for AP as well. These findings strongly suggest that AT and AP predominantly undergo reaction with the  $\text{HOO}^\bullet$  radical via the HAT mechanism.

#### 4. CONCLUSIONS

The investigation into the free radical scavenging capabilities of AT and AP involved a comprehensive approach, combining experimental techniques and quantum chemical calculations. Experimental methodologies, such as the DPPH<sup>•</sup> and ABTS<sup>•+</sup> assays, were employed to determine  $\text{IC}_{50}$  values, while theoretical analyses encompassed assessments of frontier molecular orbitals, molecular electrostatic potential, and thermodynamic parameters of reaction mechanisms. Addition-

ally, rate constant calculations were conducted to explore three mechanisms: hydrogen atom transfer (HAT), single electron transfer (SET), and radical adduct formation (RAF). The findings of this study revealed several key insights:

1. In the DPPH<sup>•</sup> assay, AT exhibited superior DPPH<sup>•</sup> radical scavenging efficacy compared to AP, as evidenced by lower  $\text{IC}_{50\text{DPPH}}$  values for AT ( $1.3 \times 10^{-3} \pm 0.2 \times 10^{-3} \text{ M}$ ) relative to AP ( $2.2 \times 10^{-3} \pm 0.1 \times 10^{-3} \text{ M}$ ).
2. In the ABTS<sup>•+</sup> test, AT demonstrated enhanced neutralization of ABTS<sup>•+</sup> free radical cations compared to AP, with calculated  $\text{IC}_{50\text{ABTS}}$  values of  $4.7 \times 10^{-5} \pm 0.1 \times 10^{-5} \text{ M}$  and  $5.5 \times 10^{-5} \pm 0.2 \times 10^{-5} \text{ M}$ , respectively.
3. Frontier molecular orbital analysis revealed that both AT and AP derivatives exhibited distributed electron transfer and acceptor regions throughout their molecular structures. Molecular electrostatic potential studies identified specific sites, particularly the hydrogen atoms within NH and  $\text{NH}_2$  groups, as favorable targets for nucleophilic attacks.
4. Thermodynamic parameter calculations indicated a preference for the HAT mechanism in the gas phase reactions of AT and AP, while the reactions in ethanol favored the SETPT and SPLET mechanisms.
5. Regarding rate constant calculations, the HAT mechanism dominated SET and RAF in reactions between AT and AP with  $\text{HOO}^\bullet$  radicals. Notably, the product quantities via the HAT mechanism accounted for over 99% of the total products in the gas phase and ethanol.
6. Both experimental and theoretical analyses collectively affirmed that AT exhibited superior antioxidant ability compared to AP, highlighting its potential as a potent free radical scavenger.

#### ■ ASSOCIATED CONTENT

##### SI Supporting Information

The Supporting Information is available free of charge at <https://pubs.acs.org/doi/10.1021/acsomega.4c02931>.

IR spectra of AT and AP; detailed instructions on calculating the rate constants for the SET, RAF, and HAT mechanisms; and Cartesian coordinates for the studied species in the gas phase and ethanol using M06–2X/6-311++g(d,p) (PDF)

#### ■ AUTHOR INFORMATION

##### Corresponding Author

Dinh Quy Huong – Department of Chemistry, University of Education, Hue University, Hue 530000, Vietnam;

orcid.org/0000-0002-2610-7151; Email: dqhuong@hueuni.edu.vn

##### Authors

Pham Cam Nam – Department of Chemical Engineering, The University of Danang – University of Science and Technology, Danang 550000, Vietnam

Duong Tuan Quang – Department of Chemistry, University of Education, Hue University, Hue 530000, Vietnam

Son Tung Ngo – Laboratory of Biophysics, Institute for Advanced Study in Technology, Ton Duc Thang University, Ho Chi Minh City 72195, Vietnam; Faculty of Pharmacy, Ton Duc Thang University, Ho Chi Minh City 72195, Vietnam; orcid.org/0000-0003-1034-1768

Tran Duong – Department of Chemistry, University of Education, Hue University, Hue 530000, Vietnam  
Nguyen Minh Tam – Faculty of Basic Sciences, University of Phan Thiet, Phan Thiet City 77000, Viet Nam

Complete contact information is available at:  
<https://pubs.acs.org/10.1021/acsomega.4c02931>

### Author Contributions

D.Q.H.: Data curation, Formal analysis, Visualization, Writing—original draft, Writing—review and editing; D.T.Q.: Data curation, Formal analysis, Visualization; P.C.N.: Supervision, Software, Writing—review and editing; N.M.T.: Supervision, Writing—review and editing; N.S.T.: Conceptualization, Methodology, Validation; T.D.: Writing—review and editing.

### Notes

The authors declare no competing financial interest.

## ACKNOWLEDGMENTS

D.Q.H. was funded by the Postdoctoral Scholarship Programme of Vingroup Innovation Foundation (VINIF), code VINIF.2023.STS.24.

## REFERENCES

- (1) Dakubo, J. C.; Naaeder, S. B.; Tettey, Y.; Gyasi, R. K. Colorectal carcinoma: an update of current trends in Accra. *West African journal of medicine* **2011**, *29* (3), 178–183.
- (2) Galano, A.; Mazzone, G.; Alvarez-Diduk, R.; Marino, T.; Alvarez-Idaboy, J. R.; Russo, N. Food Antioxidants: Chemical Insights at the Molecular Level. *Annual review of food science and technology* **2016**, *7*, 335–352.
- (3) Gulcin, I. Antioxidants and antioxidant methods: an updated overview. *Archives of toxicology* **2020**, *94* (3), 651–715.
- (4) Lourenco, S. C.; Moldao-Martins, M.; Alves, V. D. Antioxidants of Natural Plant Origins: From Sources to Food Industry Applications. *Molecules* **2019**, *24* (22), 4132.
- (5) Pachuta-Stec, A. Antioxidant Activity of 1,2,4-Triazole and its Derivatives: A Mini-Review. *Mini reviews in medicinal chemistry* **2022**, *22* (7), 1081–1094.
- (6) Hassan, G. S.; El-Messery, S. M.; Al-Omary, F. A.; Al-Rashood, S. T.; Shabayek, M. I.; Abulfadl, Y. S.; Habib el, S. E.; El-Hallouty, S. M.; Fayad, W.; Mohamed, K. M.; et al. Nonclassical antifolates, part 4. 5-(2-aminothiazol-4-yl)-4-phenyl-4H-1,2,4-triazole-3-thiols as a new class of DHFR inhibitors: synthesis, biological evaluation and molecular modeling study. *Eur. J. Med. Chem.* **2013**, *66*, 135–145.
- (7) Eswaran, S.; Adhikari, A. V.; Shetty, N. S. Synthesis and antimicrobial activities of novel quinoline derivatives carrying 1,2,4-triazole moiety. *European journal of medicinal chemistry* **2009**, *44* (11), 4637–4647.
- (8) Kuş, C.; Ayhan-Kılıçgil, G.; Özbey, S.; Kaynak, F. B.; Kaya, M.; Çoban, T.; Can-Eke, B. Synthesis and antioxidant properties of novel N-methyl-1,3,4-thiadiazol-2-amine and 4-methyl-2H-1,2,4-triazole-3(4H)-thione derivatives of benzimidazole class. *Bioorg. Med. Chem.* **2008**, *16* (8), 4294–4303.
- (9) Hamoud, M. M. S.; Osman, N. A.; Rezg, S.; A. A. Abd El-wahab, H.; E. A. Hassan, A.; Abdel-Fattah, H. A.; Romero, D. G.; Ghanim, A. M. Design and Synthesis of Novel 1,3,4-Oxadiazole and 1,2,4-Triazole Derivatives as Cyclooxygenase-2 Inhibitors with Anti-inflammatory and Antioxidant activity in LPS-stimulated RAW264.7 Macrophages. *Bioorg. Chem.* **2022**, *124*, No. 105808.
- (10) Pokuri, S.; Singla, R. K.; Bhat, V. G.; Shenoy, G. G. Insights on the antioxidant potential of 1, 2, 4-triazoles: synthesis, screening & QSAR studies. *Current drug metabolism* **2014**, *15* (4), 389–397.
- (11) Koparir, M.; Orek, C.; Parlak, A. E.; Soylemez, A.; Koparir, P.; Karatepe, M.; Dastan, S. D. Synthesis and biological activities of some novel aminomethyl derivatives of 4-substituted-5-(2-thienyl)-2,4-dihydro-3H-1,2,4-triazole-3-thiones. *European journal of medicinal chemistry* **2013**, *63*, 340–346.
- (12) Das, M.; Das, B.; Samanta, A. Antioxidant and anticancer activity of synthesized 4-amino-5-((aryl substituted)-4H-1,2,4-triazole-3-yl)thio-linked hydroxamic acid derivatives. *J. Pharm. Pharmacol.* **2019**, *71* (9), 1400–1411.
- (13) Cetin, A.; Gecibesler, I. Evaluation as antioxidant agents of 1,2,4-triazole derivatives: effects of essential functional groups. *Journal of Applied Pharmaceutical Science* **2015**, 120–126.
- (14) Cao, J.; Ren, Q.; Chen, F.; Lu, T. Comparative study on the methods for predicting the reactive site of nucleophilic reaction. *Science China Chemistry* **2015**, *58* (12), 1845–1852.
- (15) Praveena, R.; Sadasivam, K.; Deepha, V.; Sivakumar, R. Antioxidant potential of orientin: A combined experimental and DFT approach. *J. Mol. Struct.* **2014**, *1061*, 114–123.
- (16) Prasetyo, W. E.; Kurniansyah, V.; Firdaus, M.; Wibowo, F. R.; Hadda, T. B.; Almalki, F. A.; Ahmed, S. A.; Kusumaningsih, T. Free radical scavenging behaviour of the plant-beneficial secondary metabolite 2,4-diacetylphloroglucinol derivatives under physiological conditions: A joint experimental and theoretical study. *J. Mol. Struct.* **2024**, *1302*, No. 137498.
- (17) Litwinienko, G.; Ingold, K. U. Abnormal Solvent Effects on Hydrogen Atom Abstractions. 1. The Reactions of Phenols with 2,2-Diphenyl-1-picrylhydrazyl (dpph•) in Alcohols. *Journal of Organic Chemistry* **2003**, *68* (9), 3433–3438.
- (18) Xie, J.; Schaich, K. M. Re-evaluation of the 2,2-diphenyl-1-picrylhydrazyl free radical (DPPH) assay for antioxidant activity. *Journal of agricultural and food chemistry* **2014**, *62* (19), 4251–4260.
- (19) Re, R.; Pellegrini, N.; Proteggente, A.; Pannala, A.; Yang, M.; Rice-Evans, C. Antioxidant activity applying an improved ABTS radical cation decolorization assay. *Free Radic. Biol. Med.* **1999**, *26* (9–10), 1231–1237.
- (20) *Gaussian 16 Rev. B.01*; Gaussian, Inc.: Wallingford, CT, 2016.
- (21) Zhao, Y.; Truhlar, D. G. The M06 suite of density functionals for main group thermochemistry, thermochemical kinetics, non-covalent interactions, excited states, and transition elements: two new functionals and systematic testing of four M06-class functionals and 12 other functionals. *Theor. Chem. Acc.* **2008**, *120* (1–3), 215–241.
- (22) Kromann, J. C.; Steinmann, C.; Jensen, J. H. Improving solvation energy predictions using the SMD solvation method and semiempirical electronic structure methods. *J. Chem. Phys.* **2018**, *149* (10), No. 104102.
- (23) Pearson, R. G. Recent advances in the concept of hard and soft acids and bases. *J. Chem. Educ.* **1987**, *64* (7), S61.
- (24) Janak, J. F. Proof that  $\delta E/\delta n_i = \epsilon_i$  in density-functional theory. *Phys. Rev. B* **1978**, *18* (12), 7165–7168.
- (25) Rohman, R.; Nath, R.; Kar, R. Revisiting the hydrogen atom transfer reactions through a simple and accurate theoretical model: Role of hydrogen bond energy in polyphenolic antioxidants. *Computational and Theoretical Chemistry* **2023**, *1223*, No. 114097.
- (26) Wang, G.; Xue, Y.; An, L.; Zheng, Y.; Dou, Y.; Zhang, L.; Liu, Y. Theoretical study on the structural and antioxidant properties of some recently synthesised 2,4,5-trimethoxy chalcones. *Food chemistry* **2015**, *171*, 89–97.
- (27) Hossen, J.; Ali, M. A.; Reza, S. Theoretical investigations on the antioxidant potential of a non-phenolic compound thymoquinone: a DFT approach. *J. Mol. Model.* **2021**, *27* (6), 173.
- (28) Alvarez-Diduk, R.; Galano, A.; Tan, D. X.; Reiter, R. J. The key role of the sequential proton loss electron transfer mechanism on the free radical scavenging activity of some melatonin-related compounds. *Theor. Chem. Acc.* **2016**, *135* (2), 38.
- (29) Biela, M.; Rimarcik, J.; Senajova, E.; Kleinova, A.; Klein, E. Antioxidant action of deprotonated flavonoids: Thermodynamics of sequential proton-loss electron-transfer. *Phytochemistry* **2020**, *180*, No. 112528.
- (30) Marković, Z.; Tošović, J.; Milenković, D.; Marković, S. Revisiting the solvation enthalpies and free energies of the proton and electron in various solvents. *Computational and Theoretical Chemistry* **2016**, *1077*, 11–17.

- (31) Huong, D. Q.; Nam, P. C.; Duong, T. Experimental and theoretical insights into free radical capturing activity of 1,5-diaminonaphthalene and 1,5-dihydroxynaphthalene. *J. Mol. Struct.* **2023**, *1285*, No. 135537.
- (32) Marcus, R. A. Chemical and Electrochemical Electron-Transfer Theory. *Annu. Rev. Phys. Chem.* **1964**, *15* (1), 155–196.
- (33) Vo, Q. V.; Bay, M. V.; Nam, P. C.; Mechler, A. Hydroxyl Radical Scavenging of Indole-3-Carbinol: A Mechanistic and Kinetic Study. *ACS Omega* **2019**, *4* (21), 19375–19381.
- (34) Galano, A.; Alvarez-Idaboy, J. R. A computational methodology for accurate predictions of rate constants in solution: application to the assessment of primary antioxidant activity. *Journal of computational chemistry* **2013**, *34* (28), 2430–2445.
- (35) Sadiq, H.; Sadiq, H.; Sohail, A.; Basit, A.; Akhtar, N.; Batool, K.; Hisaindee, S.; Asghar, L. Assessment of antioxidant activity of pure graphene oxide (GO) and composite V<sub>2</sub>O<sub>5</sub>/GO using DPPH radical and H<sub>2</sub>O<sub>2</sub> scavenging assays. *J. Sol-Gel Sci. Technol.* **2023**, *108* (3), 840–849.
- (36) Mentese, E.; Yilmaz, F.; Baltas, N.; Bekircan, O.; Kahveci, B. Synthesis and antioxidant activities of some new triheterocyclic compounds containing benzimidazole, thiophene, and 1,2,4-triazole rings. *Journal of enzyme inhibition and medicinal chemistry* **2015**, *30* (3), 435–441.
- (37) Martinez-Morales, F.; Alonso-Castro, A. J.; Zapata-Morales, J. R.; Carranza-Álvarez, C.; Aragon-Martinez, O. H. Use of standardized units for a correct interpretation of IC<sub>50</sub> values obtained from the inhibition of the DPPH radical by natural antioxidants. *Chemical Papers* **2020**, *74* (10), 3325–3334.
- (38) Mary, C. P. V.; Vijayakumar, S.; Shankar, R. Metal chelating ability and antioxidant properties of Curcumin-metal complexes - A DFT approach. *Journal of molecular graphics & modelling* **2018**, *79*, 1–14.
- (39) De Souza Farias, S. A.; Da Costa, K. S.; Martins, J. B. L. Analysis of Conformational, Structural, Magnetic, and Electronic Properties Related to Antioxidant Activity: Revisiting Flavan, Anthocyanidin, Flavanone, Flavonol, Isoflavone, Flavone, and Flavan-3-ol. *ACS omega* **2021**, *6* (13), 8908–8918.
- (40) Abuelizz, H. A.; Taie, H. A. A.; Bakheit, A. H.; Mostafa, G. A. E.; Marzouk, M.; Rashid, H.; Al-Salahi, R. Investigation of 4-Hydrazinobenzoic Acid Derivatives for Their Antioxidant Activity: In Vitro Screening and DFT Study. *ACS omega* **2021**, *6* (47), 31993–32004.
- (41) Thakur, A.; Verma, M.; Setia, P.; Bharti, R.; Sharma, R.; Sharma, A.; Negi, N. P.; Anand, V.; Bansal, R. DFT analysis and in vitro studies of isoxazole derivatives as potent antioxidant and antibacterial agents synthesized via one-pot methodology. *Res. Chem. Intermed.* **2023**, *49* (3), 859–883.
- (42) Yakan, H.; Bakır, T. K.; Çavuş, M. S.; Muğlu, H. New  $\beta$ -isatin aldehyde-N,N'-thiocarbohydrazones: preparation, spectroscopic studies and DFT approach to antioxidant characteristics. *Res. Chem. Intermed.* **2020**, *46* (12), 5417–5440.
- (43) Safna Hussan, K. P.; Thayyil, M. S.; Rajan, V. K.; Muraleedharan, K. Experimental and density functional theory studies on benzalkonium ibuprofenate, a double active pharmaceutical ingredient. *Computational biology and chemistry* **2018**, *72*, 113–121.
- (44) Sadasivam, K.; Kumaresan, R. Antioxidant behavior of mearnsetin and myricetin flavonoid compounds—a DFT study. *Spectrochimica acta. Part A, Molecular and biomolecular spectroscopy* **2011**, *79* (1), 282–293.
- (45) Kamalarajan, P.; Irshad Ahamed, J.; Priya, R.; Valan, M. F. Spectroscopic, computational DFT, in vitro, and molecular docking investigations of newly isolated 2, 3, 9, and 10-tetrahydroacridin-3-one from the methanolic extract of nilavembu kudineer chooranam. *Res. Chem. Intermed.* **2023**, *49* (6), 2669–2690.
- (46) Pérez-Millán, T. M.; Mendoza-Castillo, D. I.; Aguayo-Villarreal, I. A.; Rojas-Mayorga, C. K.; Villanueva-Mejía, F.; Bonilla-Petriciolet, A. Application of DFT and Response Surface Models to analyze the adsorption process of basic blue 3 and reactive blue 19 dyes on sugarcane bagasse and coconut endocarp biomass. *J. Mol. Struct.* **2023**, *1287*, No. 135658.
- (47) Farrokhnia, M. Density Functional Theory Studies on the Antioxidant Mechanism and Electronic Properties of Some Bioactive Marine Meroterpenoids: Sargahydroquionic Acid and Sargachromanol. *ACS omega* **2020**, *5* (32), 20382–20390.
- (48) Boulmokh, Y.; Belguidoum, K.; Meddour, F.; Amira-Guebailia, H. Enhanced antioxidant properties of novel curcumin derivatives: a comprehensive DFT computational study. *Struct. Chem.* **2023**.
- (49) Dimitric Markovic, J. M.; Pejin, B.; Milenkovic, D.; Amic, D.; Begovic, N.; Mojovic, M.; Markovic, Z. S. Antiradical activity of delphinidin, pelargonidin and malvin towards hydroxyl and nitric oxide radicals: The energy requirements calculations as a prediction of the possible antiradical mechanisms. *Food chemistry* **2017**, *218*, 440–446.
- (50) Chen, Y.; Xiao, H.; Zheng, J.; Liang, G. Structure-thermodynamics-antioxidant activity relationships of selected natural phenolic acids and derivatives: an experimental and theoretical evaluation. *PLoS one* **2015**, *10* (3), No. e0121276.
- (51) Anitha, S.; Krishnan, S.; Senthilkumar, K.; Sasirekha, V. Theoretical investigation on the structure and antioxidant activity of (+) catechin and (–) epicatechin – a comparative study. *Mol. Phys.* **2020**, *118* (17), No. e1745917.
- (52) Holtomo, O.; Nsangou, M.; Fifen, J. J.; Motapon, O. DFT study of the effect of solvent on the H-atom transfer involved in the scavenging of the free radicals (•)HO<sub>2</sub> and (•)O<sub>2</sub>(–) by caffeic acid phenethyl ester and some of its derivatives. *J. Mol. Model.* **2014**, *20* (11), 2509.
- (53) Xue, Y.; Chen, M.; Li, Z.; Zhang, L.; Wang, G.; Zheng, Y.; An, L. Effects of hydroxyl group, glycosylation and solvents on the antioxidant activity and mechanism of maclurin and its derivatives: Theoretical insights. *J. Mol. Liq.* **2022**, *351*, No. 118609.
- (54) Dzib, E.; Cabellos, J. L.; Ortiz-Chi, F.; Pan, S.; Galano, A.; Merino, G. Eyringpy: A program for computing rate constants in the gas phase and in solution. *Int. J. Quantum Chem.* **2019**, *119* (2), No. e25686.
- (55) Huong, D. Q.; Van Truong, D.; Tam, N. M.; Nam, P. C. Effect of hydroxyl position on antioxidant ability of hydroxycoumarin derivatives: A theoretical investigation. *J. Mol. Liq.* **2023**, *391*, No. 123312.